

# Design, fabrication and analysis of a body-caudal fin propulsion system for a microrobotic fish

Kyu-Jin Cho, Elliot Hawkes, Chris Quinn, Robert J. Wood

**Abstract**—In this paper, we present the design and fabrication of a centimeter-scale propulsion system for a robotic fish. The key to the design is selection of an appropriate actuator and a body frame that is simple and compact. SMA spring actuators are customized to provide the necessary work output for the microrobotic fish. The flexure joints, electrical wiring and attachment pads for SMA actuators are all embedded in a single layer of copper laminated polymer film, sandwiched between two layers of glass fiber. Instead of using individual actuators to rotate each joint, each actuator rotates all the joints to a certain mode shape and undulatory motion is created by a timed sequence of these mode shapes. *Subcarangiform* swimming mode of minnows has been emulated using five links and four actuators. The size of the four-joint propulsion system is 6mm wide, 40 mm long with the body frame thickness of 0.25mm.

**Index Terms**- Robotic Fish Fin, SMA spring actuator, Micro-robot

## I. INTRODUCTION

This paper describes a propulsion system for a micro robotic fish. Applications of such devices include environmental monitoring, surveillance, and in vivo diagnosis. As a starting point for our design, we will identify key physiological and morphological parameters of appropriately sized fish.

Studies have identified several types of locomotion that fish use to generate thrust [1]. Most fish generate thrust by bending their bodies into a backward-moving propulsive wave that extends to the caudal fin, a type of swimming classified under body and/or caudal fin (BCF) locomotion. The propulsive wave traverses the fish body in a direction opposite to the overall movement and at a speed greater than the overall swimming speed. There are four undulatory BCF locomotion modes identified by their amplitude envelope of the propulsive wave: *anguilliform*, *subcarangiform*, *carangiform* and *thunniform*. Despite these labels placed by biologists, two-dimensional analyses of fish locomotion have shown that even fishes of very different body types show extremely similar patterns of body movement when viewed in a horizontal section during steady undulatory locomotion [2]. Nevertheless, *subcarangiform* swimming mode is the basis of the undulatory motion created by our robotic fish. *Subcarangiform* locomotion is the mode of undulatory

swimming used by minnows in which waves are propagated posteriorly along the length, propelling it forward.

Large scale robotic fish have been built by several researchers. Willy [3] describes a robotic fin to emulate the anguilliform and Morgansen [4], [5] describes a robotic testbed for the study of carangiform swimming, while the MIT RoboTuna is an example of a robotic thunniform swimmer [6].

An actuator for a minnow-size robotic fish has to be compact and lightweight while providing sufficient displacement and force to deflect fin sections to a desired angle at an operational speed of 2-4 Hz, durable enough to operate thousands of cycles, low cost, and easy to assemble. Some of the actuators that were considered for this role include ionic polymer metal composites (IPMCs), dielectric elastomers, piezoelectrics, and shape memory alloys. IPMCs have been used extensively for water based robotics [7], [8], as their need to be immersed in an ion-rich fluid makes them a natural choice. Dielectric elastomers are notable for being employed in a large number of geometries and for having very large deformations [7]. Both piezoelectric ceramics and polymers are well known for being capable of operating above 1kHz at moderate voltages, and the ceramics can also generate large stresses [8]. Fukuda *et al.* have used pair of PZT actuators along with an amplification mechanism for a swimming microrobot [9]. Shape memory alloy (SMA) actuators have large energy density, a unique two-phase (martensite/austenite) property, and have actuated robotic hands [10], crawling microrobots [11], and several robotic fish fins [12], [13], [14], [15].

Our choice of SMA spring actuation was based on the large space of force and displacement this morphology will allow. Furthermore, these materials are resilient and easy to handle and fabricate.

Using a novel SMA spring design and a flexure-based skeleton, we are able to build the smallest multi-segmented robotic fish fin using SMA actuators to date. This device has five 6mm square segments that are 250  $\mu\text{m}$  thick and four SMA spring actuators 200  $\mu\text{m}$  in diameter. At this scale, joints are made using flexures. Electrical wiring, as well as the attachment of SMA springs, is simplified by a patterned copper-laminated polymer film that is used for the flexure material. While this design is for a small DOF fin, it will be easily iterated for large DOF swimming fish, as actual fish locomotion is quite complex.

This work was supported by the Harvard University Center for the Environment.

K. Cho, E. Hawkes and R.J. Wood are with the Microrobotics Laboratory, School of Engineering and Applied Sciences, Harvard University. C. Quinn is with the Department of Applied and Engineering Physics, Cornell University. e-mail: rjwood@eeecs.harvard.edu

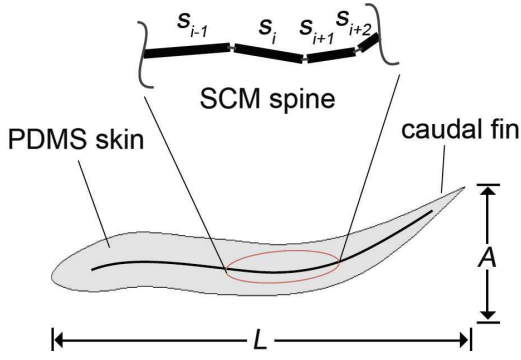


Fig. 1. The concept of a BCF propulsion mechanism is based upon a novel 'meso'-scale manufacturing paradigm called smart composite microstructures[16]. In this concept the spine is created with a sequence of rigid links separated by flexure joints.

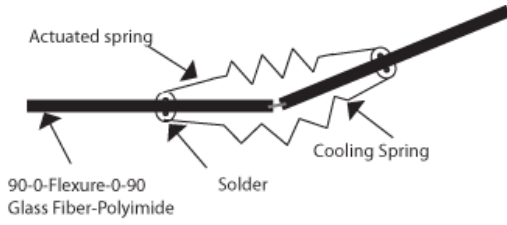


Fig. 2. The basic concept uses antagonistic actuation at each joint.

## II. DESIGN

### A. Basic Concept

The basic concept of the microrobotic fish is displayed in Fig. 1 and is composed of a flexure-jointed composite fiber spine that will be covered with a PDMS skin. The motion of the caudal fin is driven by the SMA springs attached on either side of each flexure(see Fig. 2). These are actuated in succession to create a traveling waveform.

### B. Actuator Selection

In past iterations of the BCF propulsion mechanism, straight SMA wires were used with little success since the force generated by the wire was too large to allow for a robust attachment. The spring was adopted as it not only decreases the surplus of force, but also increases deflection, allowing for well over 100% strain. This excess strain creates more motion in the tail and allows for ease in mounting, as the spring can be stretched, attached, then actuated to return to working length. The design of the spring has multiple parameters that must be considered based on the deflection of the spring,  $\delta$ , and the spring constant,  $k$ , which are given as follows[17]:

$$\delta = \frac{8PD^3n}{Gd^4} \quad (1)$$

$$k = \frac{Gd^4}{8D^3n} \quad (2)$$

where  $D$  is the spring diameter measured from center of wire on either side,  $d$  is the wire diameter,  $n$  is the number

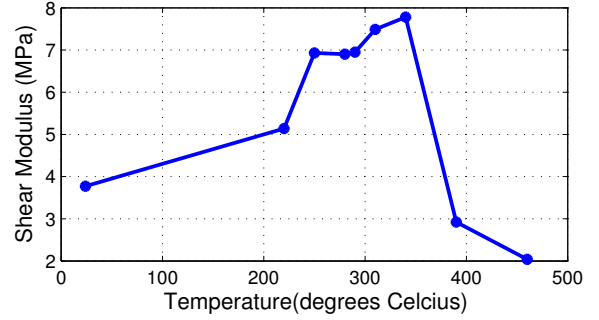


Fig. 3. The shear modulus of the SMA can be adjusted by choice of annealing temperature.

of active coils in the spring,  $P$  is the load, and  $G$  is the shear modulus of SMA wire after annealing.

Thus to adjust our spring constant  $k$ , we had three parameters to choose from:  $d$ ,  $D$ , and  $n$ . We would like to minimize  $d$  as this decreases cooling time, and  $n$  was limited by the length of spring needed. Therefore we were left with  $D$  to minimize as much as possible without decreasing the deflection outside of a useful range. Therefore a spring index,  $D/d$ , was chosen between 2.5 and 3.

However, one more parameter can be altered, namely  $G$ , the shear modulus. The value of  $G$  for the austenite phase of a spring is around 3.77 MPa when the wire is plastically deformed into a coil and not annealed. This value can be increased to almost 7.8 MPa when annealed (see Fig. 3). By annealing slightly above 300 degrees (measured externally with a thermocouple-actual internal temperature is higher) we were able to maximize the shear modulus. By understanding the annealing process and the model in eq. (1) and eq. (2), we are able to choose the geometry that gives us the desired stress and strain required to achieve the individual flexure motion.

### C. Flexure Design

The flexures are designed to avoid buckling under normal operation while remaining sufficiently compliant (compared with the actuator stiffness). Flexures are made with a custom process using thin-film polymers sandwiched between rigid composite plates [16]. Polymers are chosen for resilience and high elastic strain limit (allowing large motions with compact geometries) [18]. However, in this case, current needs to be passed through each flexure to power more distal actuators on adjacent segments. To accomplish this, we used patterned copper laminated on a thin-film polymer. Therefore, we must take special care in designing the flexure geometry to avoid plastic deformations while keeping the stiffness low. To start, the pseudo-rigid-body model of a compliant mechanism assumes that the flexure can be conceptually replaced by a perfect pin joint in parallel with a rotational flexure. The spring constant of this flexure is:

$$k_{\theta} = \frac{EI}{L} \quad (3)$$

Since this is a composite beam, we need to determine the effective modulus and the second moment of area of the flexure to use in eq. 3. This is done using a standard transformation for a composite beam. First, the width of the polymer section,  $w_p$  is multiplied by a factor  $n$  which is the ratio of the modulus of the polymer to the modulus of the conductor ( $n = E_p/E_c$ ). This results in a transformed homogeneous beam with modulus  $E_c$ . Determining the second moment of area of this beam takes two steps: 1) determine the location of the neutral axis, and 2) use this neutral axis and the parallel axis theorem to calculate the second moment of area. Since the transformed area can be broken down into two rectangular areas, the location of the neutral axis is defined as follows:

$$\bar{Y} = \frac{\sum \bar{y}_i A_i}{\sum A_i} = \frac{(h_p + h_c/2) w_c h_c + (h_p/2) n w_p h_p}{w_c h_c + n w_p h_p} \quad (4)$$

where  $\bar{y}_i$  are the distances from the bottom edge of the beam to the centroid of each area and  $A_i$  is the area of each section. The second moment of area is now found as:

$$I' = \sum \frac{w_i h_i^3}{12} + A_i d_i^2 = \frac{w_c h_c^3}{12} + w_c h_c (\bar{y}_c - \bar{Y})^2 + \frac{n w_p h_p^3}{12} + n w_p h_p (\bar{y}_p - \bar{Y})^2 \quad (5)$$

Now the terms  $E_c$  and  $I'$  can replace  $E$  and  $I$  in eq. 3 respectively. Next, we are interested in the maximum deflection allowed by the strain limit of the flexure materials. This will be limited by the conductor, so we will only present calculations based upon the copper layer. From simple beam theory, the maximum strain in a bending beam is related to the beam deflection as follows:

$$\theta_{max} = \frac{L \epsilon_{max}}{(h_c + h_p - \bar{Y})} \quad (6)$$

where  $\epsilon_{max}$  is the yield strain of copper. For a 1mm wide, 12 $\mu$ m thick copper conductor laminated on 5.75mm wide, 12.7 $\mu$ m thick polyimide, the rotational stiffness is < 0.25mNm/rad. This flexure can achieve >  $\pm 10^\circ$  of motion without plastic deformation. However, we must also consider beam buckling due to the axial loads from the SMA actuators. The Euler buckling criterion for this flexure morphology is given as:

$$F_{max} = \frac{\pi^2 E_c I'}{(0.5L)^2} \quad (7)$$

Therefore, this flexure can withstand >20N before buckling. In the case where this buckling strength is insufficient, we can use alternative flexure designs such as an inversion flexure [19].

#### D. Generating Motion

By coordinating the rotation of each joint, undulatory motion can be created. A common method to create these motions is to drive each joint with an individual actuator and coordinate these rotations. However, we have designed our system so that a single mode can be created with a single

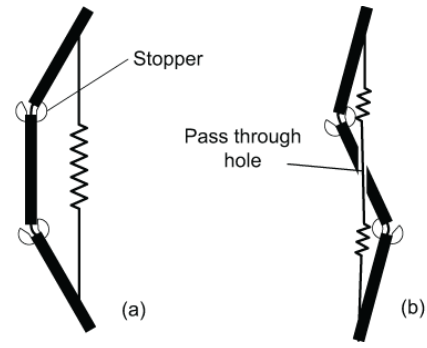


Fig. 4. Basic building blocks for motion creation: (a) C-type (b) S-type.

actuator, where each mode would represent a certain shape of the tail. A timed sequence of multiple modes would create an undulatory motion. This method simplifies the control and design of the system since it requires a single input to control multiple joints for a certain mode.

A single mode can be created by connecting two basic building blocks in series. Each building block is composed of multiple segments with an actuator fixed at the two end segments. Every joint has a mechanical stopper that defines the angle of each joint when the actuator is activated.

Fig. 4 shows the two basic building blocks. C-type is created by having the actuator on one side, with the actuators fixed at the two end segments. S-type is created by having an actuator fixed at one end, passing through the hole in the middle segment, and connecting at the last segment on the opposite side. The angle of the stopper limits the rotation angle of the joints and defines the shape. The actuator should be able to generate enough force and displacement to rotate the joints until all the stoppers touch the adjoining segments. As long as the actuator passes through an attachment point of each segment, there would be a single mode that can be created by the activation of the actuator. Variation of these two building blocks can be created by changing the number and the length of segments and the stopping angles of each joint. Combining a mix of these two building blocks in series creates various mode shapes, each activated by a single actuator.

We have created *subcarangiform* swimming mode by using the two basic building blocks discussed above. Fig. 5 shows the resulting motion. There are two basic modes, where each mode has an antagonistic version. Modes (a) and (c) are series combination of two C-types and modes (b) and (d) are series combination of two S-types. The actuator shown on each mode is a single actuator connected from one end to the other. The four modes are activated with a sequence of (a) to (d), and repeating the sequence creates a continuous motion. Four actuators are connected to the body frame, one for each mode. They should provide enough force and displacement when activated to create each mode, but should also be able to be elongated when other actuators are activated to create other modes. Again, this is a benefit of SMA coil actuators as opposed to straight SMA actuator

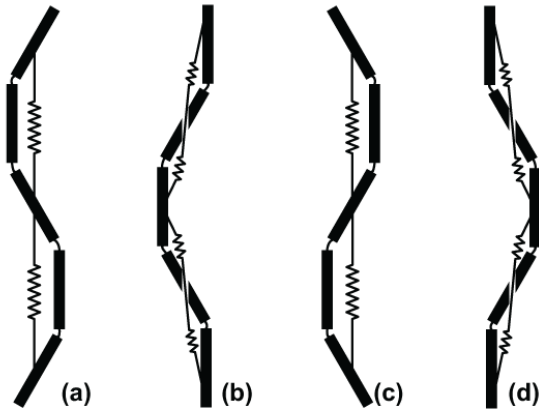


Fig. 5. Subcarangiform BCF motion is created with four modes. Notice a traveling wave created as each mode is sequentially activated from (a) to (d).

wires.

### III. FABRICATION

#### A. SMA Coil Actuator Annealing

In order to achieve a spring-like geometry for a shape memory alloy, a high temperature annealing process is used. The annealing process begins by stretching a wire 2.5-3 times the diameter of the SMA wire between two adjustable clamps. Two loops are then tied in either end of the SMA, one of which is hooked onto an anchor attached to the near clamp and the other connected to a clip that is used as a handle for winding. Depending on the length of the spring, the SMA wire is wound around the support wire 10-20 times, keeping the coil tight and closed (no space between loops). Multiple springs can be made on a single wire. Fig. 6-(a) shows the SMA wire wound around a conducting mold wire for the annealing process. The number of springs, and spacing between them are customized based on the force and displacement requirements and geometrical considerations. For the robotic fish, four springs with a wire diameter of  $760\mu\text{m}$ , each with 17 windings are wrapped with a spacing of about 0.8mm between each spring. After wrapping, the clip is attached to the clamp and a weight is hung to keep tension as the support wire deforms. Current is run through the mold wire until the desired temperature is attained (read from a thermocouple). The lead wire is cut and the springs are slid off and tested before use. Fig. 6-(b) shows two sets of springs, one before stretching and the other one stretched and ready to be attached to the body frame.

#### B. Spine and Flexure Fabrication

To overcome the limitations with traditional macro-scale manufacturing techniques for sub-millimeter scale articulated devices, we have developed a meso-scale rapid prototyping method called Smart Composite Microstructures (SCM) [16]. This process entails the use of laminated, laser-micromachined materials stacked to achieve a desired compliance profile. Fig. 7 gives an overview of the SCM

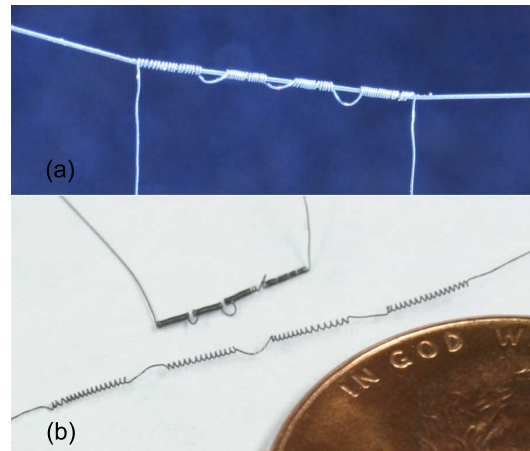


Fig. 6. Annealing of SMA spring actuators. (a) SMA wire is wound around a conducting 'mold' wire which heats the SMA wire during annealing. (b) Annealed SMA springs, unstretched and stretched (penny is shown at the bottom right side for size comparison).

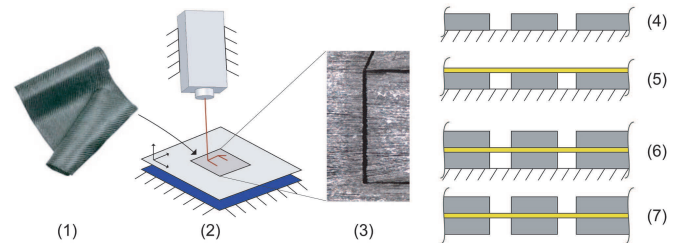


Fig. 7. Overview of the laser micromachining step of the SCM process. First, composite prepreg(1) and thin-film polymer laminae are laser cut(2) to desired planform geometries(3). These laminae are then aligned, stacked(5-6), and cured to form the spine segments(7).

process that is used to create the links and joints of the microrobotic fish spine.

A new method of using copper-laminated foils as the flexure material, electrical connection, and mechanical attachment points for the SMA actuators was developed. Copper-laminated polyimide foil is used as the flexure layer, with two perpendicularly aligned glass fiber layers laminated on both sides. The copper foil is masked using kapton tape and a pattern is created using a laser cutter (Versa Laser VLS3.5). The tape is peeled off from the sections to be etched with a ferric chloride solution. To align the features precisely, the polyimide layer is etched twice. First the regions that are to be cut through are etched, and a pattern for the copper area is created with the laser cutter on the etched polyimide layer. Then it is etched again to create the final shape. Fig. 8 shows the fabricated polyimide layer.

Two single layer glass fiber laminae are joined orthogonally, and cut with a laser. Two of these are cured with the patterned copper-laminated polyimide to create the spine or the body frame. Fig. 9 shows the body frame with four flexure joints, electrical wiring and the SMA attachment pads as well as positioning holes needed to assemble the stoppers.

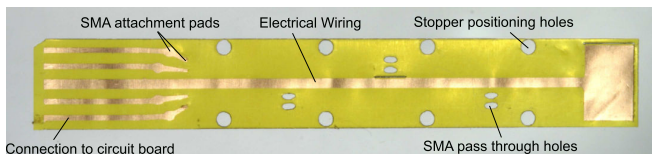


Fig. 8. Copper-laminated polyimide layer patterned and etched to accommodate electrical wiring and attachment points for the SMA actuators.

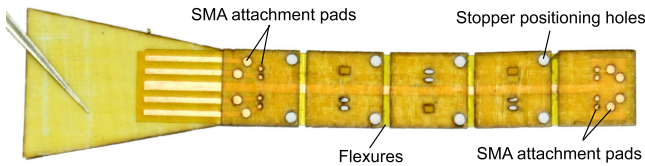


Fig. 9. Four-segment spine with electrical wiring, actuator attachment pads, stopper positioning holes and flexures.

### C. Assembly

Fig. 10 shows the assembled robotic fish fin with four joints. The stoppers that define the joint angles are fabricated using a rapid prototyping machine (Invision SR from 3D systems) with a plastic material (Visijet SR200). The stoppers are built as a mating set: one with pegs and the other with holes. They are attached on both sides of each joint through the positioning holes with epoxy. The stopping angle is 25 degrees, and the height is 1.5mm. The SMA actuators are soldered on the copper attachment pads with a sulfuric acid based liquid flux and a silver bearing solder. This provides electrical contacts as well as mechanical connections. The actuators either pass through a hole at the center of each segment, or they pass under a hook (made of glass fiber) to make sure they are positioned on top of the segments. The total length of the four joint fish fin is 40mm, with a height of 6 mm. The thickness of the frame is approximately 250 microns.

## IV. RESULTS

In order to characterize the robotic fish fin, a single joint with a size of 1cm by 1cm with a SMA coil actuator with

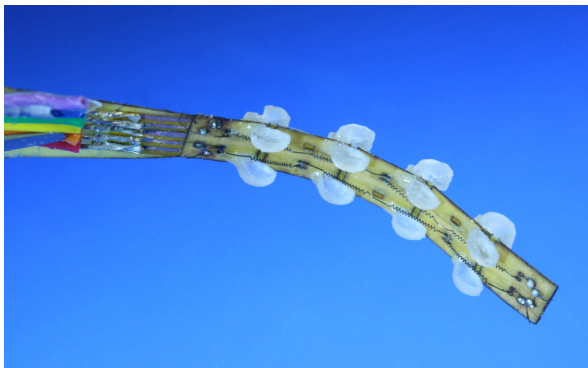


Fig. 10. Completed robotic fish fin with four joints.

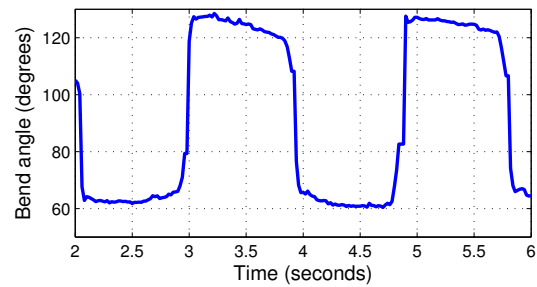


Fig. 11. Antagonistic activation characteristics for a single joint.

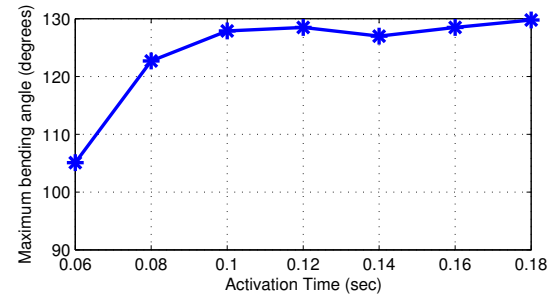


Fig. 12. Maximum bending angle for various activation times.

a diameter of 100  $\mu\text{m}$  was built and tested. It is driven by two MOSFETs, which are controlled using MathWorks xPC target real time control software. The motion is captured with a video camera to analyze the bending angle of the joints. Fig. 11 shows an example of bending angle vs. time as we activate the spring SMA actuator with 0.6 A for 0.12 sec, rest for 0.8 sec, then activate the antagonistic actuator. In order to choose the amount of activation time for a given current we ran a series of trials where the time interval is compared to maximum bending angle (e.g. see Fig. 12 for 0.6 A). For each current we choose the time at which the saturation point is reached, thus minimizing power input and preventing overheating.

Energy efficiency increases with increasing current since the activation time decreases which also decreases the amount of heat loss during activation. As displayed in Fig. 13, the activation time decreases exponentially with increasing current. But the current amplitude will be limited by the power supply that will eventually be on board.

To activate a 100  $\mu\text{m}$  wire diameter SMA spring actuator, current of 0.6 A is needed at 1.09 V. To get a maximum bending angle, 0.12 seconds is needed. Since a single cycle requires the activation of two antagonistic actuators, 0.15W are consumed per cycle. With a Lithium Polymer battery rated at 20mAh with 3.7V nominal output and weight of 1gram (Kokam SLB455018), about 1696 cycles can be performed, assuming that the losses from other electronic components are minimal. For a 2 Hz motion, this corresponds to a continuous operation time of around 14 minutes.

The final robotic fish fin has been tested to activate each mode shown in fig. 5. Each mode is created by activating the

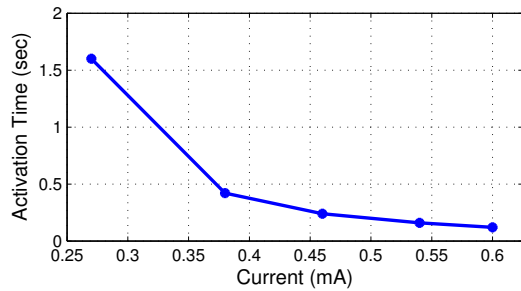


Fig. 13. Activation time decreases exponentially with the magnitude of current applied to the actuator.

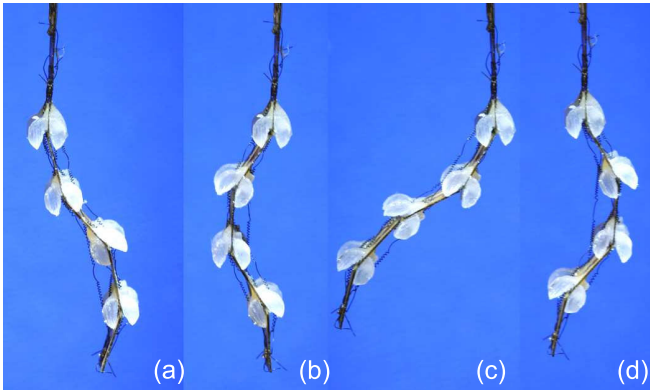


Fig. 14. Sequential activation of the four modes of the BCF propulsion mechanism.

four actuators in sequence. There are few things that need to be carefully considered. The actuators need to move freely in the pass-through holes when changing from one mode to the other, and sufficient moment is needed to pull the segments that are bent in the other direction in the previous mode. Fig. 14 shows the resulting shapes from an initial experiment of activating each mode.

## V. SUMMARY AND FUTURE WORK

In this paper, a body caudal fin propulsion system using SMA spring actuators mounted on a multi-segmented, flexure based frame has been presented. Eventually, the fish will be built with integrated electronics and covered with a protective skin.

The design and fabrication techniques presented are simple, robust, and scalable. By customizing the SMA spring actuator, we can create an actuated flexure joint with a range of displacements and forces, instead of a set amount of strain and force that straight wire SMA actuators provide. Flexures, electrical wiring, and actuator attachment points are all embedded into a copper-laminated polyimide foil patterned with copper traces, solder pads and other features needed for assembly. This simplicity in design and fabrication, as well as the fact that the actuator characteristics can be customized, makes this device a very good candidate for a backbone of various other small-scale robots. Undulatory motion is created by using a sequence of mode shapes. This

scheme of using a single actuator to create a single mode that coordinates multiple joint angles further simplifies the design and control of the device.

Much progress can be made on both the design and control of the robot. Varying each segment length to fit the natural motion of a fish as well as increasing total number of segments will result in a more realistic tail motion. Control of this motion will also be optimized using PWM, allowing for concurrent actuation and thus smoother motion.

## REFERENCES

- [1] M. Sfakiotakis, D. Lane, and J. Davies, "Review of fish swimming modes for aquatic locomotion," *J. of Oceanic Engineering*, vol. 24, no. 2, pp. 237–252, 1999.
- [2] E. D. T. G. V. Lauder, *Fish Biomechanics*. San Diego: Academic Press, 2006, vol. 23, ch. Hydrodynamics of Undulatory Propulsion, pp. 425–468.
- [3] A. Willy and K. H. Low, "Development and initial experiment of modular undulating fin for untethered biorobotic AUVs," in *2005 Proc. IEEE Int. Conf. Robotics and Biomimetics (ROBIO)*, pp. 45–50.
- [4] K. Morgansen, V. Duindam, R. Mason, J. Burdick, and R. Murray, "Nonlinear control methods for planar carangiform robot fish locomotion," in *2001 Proc. IEEE Int. Conf. Robotics and Automation*, pp. 427–343.
- [5] K. Morgansen, P. Vela, and J. Burdick, "Trajectory stabilization for a planar carangiform robot fish," in *2002 Proc. IEEE Int. Conf. Robotics and Automation*, pp. 756–762.
- [6] G. S. Triantafyllou, M. S. Triantafyllou, "An efficient swimming machine," *Sci. Amer.*, pp. 64–70, 1995.
- [7] R. Kornbluh, R. Pelrine, J. Eckerle, and J. Joseph, "Electrostrictive polymer artificial muscle actuators," in *1998 Proc. IEEE Int. Conf. Robotics and Automation*, vol. 3, pp. 2147–2154.
- [8] Y. Fu, E. C. Harvey, M. K. Ghantasala, and G. M. Spinks, "Design, fabrication and testing of piezoelectric polymer PVDF microactuators," *Smart Materials & Structures*, vol. 15, no. 1, pp. 141–146, 2006.
- [9] T. Fukuda, T. Fukuda, A. Kawamoto, F. Arai, and H. Matsuura, "Mechanism and swimming experiment of micro mobile robot in water," in *1994 Proc. IEEE Int. Conf. Robotics and Automation*, A. Kawamoto, Ed., vol. 1, pp. 814–819.
- [10] K.-J. Cho and H. Asada, "Multi-axis SMA actuator array for driving anthropomorphic robot hand," in *2005 Proc. IEEE Int. Conf. Robotics and Automation*, pp. 1356–1361.
- [11] B. Trimmer, A. Takesian, B. Sweet, C. Rogers, D. Hake, and D. Rogers, "Caterpillar locomotion: A new model for soft-bodied climbing and burrowing robots," in *7th Int. Symp. Technology and the Mine Problem*, 2006.
- [12] N. Ono, M. Kusaka, M. Taya, and C. Wang, "Design of fish fin actuators using shape memory alloy composites," in *2004 Proc. SPIE*, vol. 5388, pp. 305–312.
- [13] O. K. Rediniotis, L. N. Wilson, D. C. Lagoudas, and M. M. Khan, "Development of a shape-memory-alloy actuated biomimetic hydrofoil," *J. of Intelligent Material Systems and Structures*, vol. 13, no. 1, pp. 35–49, 2002.
- [14] N. Shinjo and G. W. Swain, "Use of a shape memory alloy for the design of an oscillatory propulsion system," *IEEE Journal of Oceanic Engineering*, vol. 29, no. 3, pp. 750–755, 2004.
- [15] Z. Yonghua, L. Shangrong, M. Ji, and Y. Jie, "Development of an underwater oscillatory propulsion system using shape memory alloy," in *2005 IEEE Int. Conf. Mechatronics and Automation*, vol. 4, pp. 1878–1883.
- [16] R. Wood, S. Avadhanula, R. Sahai, E. Steltz, and R. Fearing, "Micro-robot design using fiber reinforced composites," *J. of Mechanical Design*, May 2008.
- [17] K. Otsuka and C. M. Wayman, *Shape Memory Materials*. Cambridge, UK: Cambridge University Press, 1998.
- [18] S. Avadhanula and R. Fearing, "Flexure design rules for carbon fiber micro-robotic mechanisms," in *2005 Proc. IEEE Int. Conf. Robotics and Automation*, pp. 1579–1584.
- [19] R. Wood, S. Avadhanula, M. Menon, and R. Fearing, "Micro-robotics using composite materials: The micromechanical flying insect thorax," in *2003 Proc. IEEE Int. Conf. Robotics and Automation*, vol. 2, pp. 1842–1849.